Muon $g-2$ and the B-physics anomalies in RPV supersymmetry and the discovery prospect at LHC and future colliders

Fang Xu

Collaborators: Bhupal Dev, Amarjit Soni
arXiv:2106.15647

SUSY 2021

Washington University in St. Louis

August 27, 2021

Overview

1. Introduction
   - Motivation
   - $(g-2)_\mu$, $R_{D^{(*)}}$ and $R_{K^{(*)}}$ Anomalies
   - Explanation in RPV3 SUSY
2. Parameter space and benchmark scenarios
   - Numerical scan
   - Benchmark scenarios
3. Simulation and results
   - Collider signals
   - Anomalies and constraints in parameter space
4. Discussion and conclusions

Motivation

- The recent experimental results of muon $g-2$ (from the Fermilab) and the lepton flavor universality violation in rare B-meson decays (from the LHCb, Belle, BaBar) could be the hints ($> 3\sigma$ anomalies) of new physics beyond the Standard Model.
- Under the minimal RPV supersymmetric framework, assuming the mass of third generation sfermions lighter than the other two generations (called "RPV3", Altmannshofer, Dev, Soni (PRD 2017)),

  muon $g-2$ and the B-physics anomalies could be addressed simultaneously and also could be tested at LHC and beyond.

muon $g-2$ anomaly

- $\Delta a_\mu = a_\mu^{\text{exp}} - a_\mu^{\text{SM}} = (251 \pm 59) \times 10^{-11}$ has a significance of 4.2σ.
- Could be the signal of new physics beyond the SM where some new couplings to muon could be detectable by LHC or future colliders.

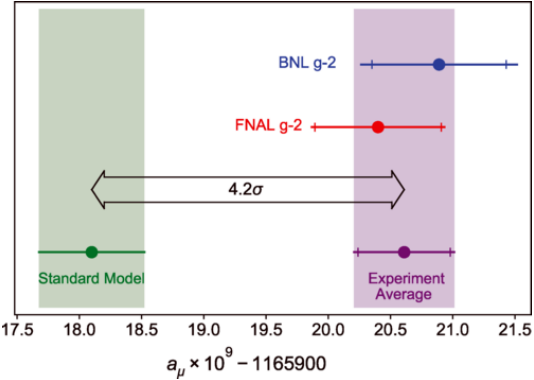

B. Abi et al. (PRL 2021)

B-physics anomalies

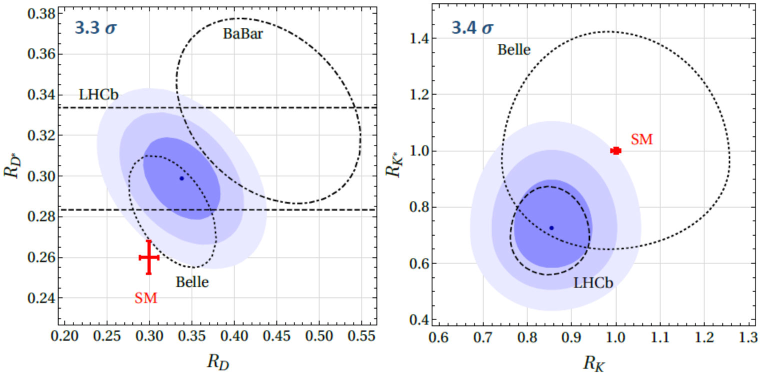

Altmannshofer, Dev, Soni, Sui (PRD 2020)

- $R_{D^{(*)}} = \frac{\text{BR}(B \to D^{(*)}\tau\nu)}{\text{BR}(B \to D^{(*)}\ell\nu)}$ (with $\ell = e, \mu$), $R_{K^{(*)}} = \frac{\text{BR}(B \to K^{(*)}\mu^+\mu^-)}{\text{BR}(B \to K^{(*)}e^+e^-)}$
- Also imply possible new couplings to leptons.

Explanation of anomalies in RPV3 SUSY

- The LQD and LLE part of the RPV SUSY Lagrangian which contains the λ' and λ couplings respectively and are relevant for the $R_{D^{(*)}}$, $R_{K^{(*)}}$ and $(g-2)_\mu$ anomalies.

$$\begin{aligned}\mathcal{L}_{LQD} = \lambda'_{ijk}(&\widetilde{\nu}_{i\mathrm{L}}\overline{d}_{k\mathrm{R}}d_{j\mathrm{L}} + \widetilde{d}_{j\mathrm{L}}\overline{d}_{k\mathrm{R}}\nu_{i\mathrm{L}} + \widetilde{d}^*_{k\mathrm{R}}\overline{\nu}^c_{i\mathrm{L}}d_{j\mathrm{L}} \\ &- \widetilde{e}_{i\mathrm{L}}\overline{d}_{k\mathrm{R}}u_{j\mathrm{L}} - \widetilde{u}_{j\mathrm{L}}\overline{d}_{k\mathrm{R}}e_{i\mathrm{L}} - \widetilde{d}^*_{k\mathrm{R}}\overline{e}^c_{i\mathrm{L}}u_{j\mathrm{L}}) + \mathrm{H.c.}\end{aligned} \tag{1}$$

$$\mathcal{L}_{LLE} = \frac{1}{2}\lambda_{ijk}\left[\widetilde{\nu}_{i\mathrm{L}}\overline{e}_{k\mathrm{R}}e_{j\mathrm{L}} + \widetilde{e}_{j\mathrm{L}}\overline{e}_{k\mathrm{R}}\nu_{i\mathrm{L}} + \widetilde{e}^*_{k\mathrm{R}}\overline{\nu}^c_{i\mathrm{L}}e_{j\mathrm{L}} - (i \leftrightarrow j)\right] + \mathrm{H.c.} \tag{2}$$

- Following previous discussions (Kim, Kyae, Lee (PLB 2001); Altmannshofer, Dev, Soni, Sui (PRD 2020)), in RPV3 framework, $(g-2)_\mu$ correction can be written as:

$$\Delta a_\mu = \frac{m_\mu^2}{96\pi^2}\sum_{k=1}^{3}\left(\frac{2(|\lambda_{32k}|^2 + |\lambda_{3k2}|^2)}{m^2_{\widetilde{\nu}_\tau}} - \frac{|\lambda_{3k2}|^2}{m^2_{\widetilde{\tau}_\mathrm{L}}} - \frac{|\lambda_{k23}|^2}{m^2_{\widetilde{\tau}_\mathrm{R}}} + \frac{3|\lambda'_{2k3}|^2}{m^2_{\widetilde{b}_\mathrm{R}}}\right) \tag{3}$$

Explanation of anomalies in RPV3 SUSY

$(g-2)_\mu$ Kim, Kyae, Lee (PLB 2001)

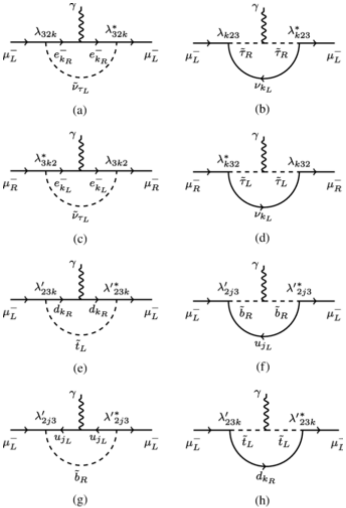

$R_{D^{(*)}}$ Deshpande, He (EPJC 2017); Altmannshofer, Dev, Soni (PRD 2017) etc.

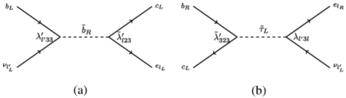

$R_{K^{(*)}}$ Das, Hati, Kumar, Mahajan (PRD 2017); Trifinopoulos (EPJC 2018) etc.

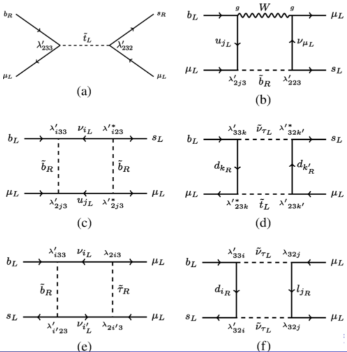

Parameter space

- Parameters $(\lambda_{232}, \lambda'_{233}, \lambda'_{223}, \lambda'_{232}, m_{\tilde{b}_\mathrm{R}}, m_{\tilde{b}_\mathrm{L}}, m_{\tilde{\nu}_\tau}, m_{\tilde{\tau}_\mathrm{L}})$
  - $\lambda_{232} = -\lambda_{322} \neq 0 \Leftarrow$ contribute to muon $g-2$, other λ_{3ij} couplings cannot be large at the same time due to the constraints of $\tau \to \mu\mu\mu$, $\mu \to e\gamma$ etc.
  - $\lambda'_{2ij} \neq 0 \Leftarrow$ include μ and free of $m_{\tilde{\nu}_\tau}$.
  - $\lambda'_{3ij} = 0$, otherwise combined with λ_{32k} or λ_{3k2}, well measured meson decays $(\bar{d}_i d_j) \to \mu\ell_k$ or $\tau \to \mu K$ and $\tau \to \mu\eta$ decays will prevent λ'_{3ij} to be large.
  - $m_{\tilde{\tau}_\mathrm{R}}$ not involved with this choice of couplings.
  - $m_{\tilde{t}_\mathrm{L}}$ can only influence $\mathrm{BR}(B_s \to \mu^+\mu^-)$ and the Wilson coefficients $(C'_9)^\mu$ and $(C'_{10})^\mu$ that describe the $R_{K^{(*)}}$ anomaly. But we can assume a relatively larger value to make the influence small.

Parameter space

- 8-D parameter space $(\lambda_{232}, \lambda'_{233}, \lambda'_{223}, \lambda'_{232}, m_{\tilde{b}_R}, m_{\tilde{b}_L}, m_{\tilde{\nu}_\tau}, m_{\tilde{\tau}_L})$
  - $m_{\tilde{b}_R} = m_{\tilde{b}_L}$ for simplicity.
  - $m_{\tilde{\tau}_L}$ has opposite contribution for $(g-2)_\mu$. The influence is not important as long as $m_{\tilde{\tau}_L} \gtrsim O(2\ \mathrm{TeV})$. Here we choose 4 TeV.
- $\Rightarrow$ 6-D parameter space $(\lambda_{232}, \lambda'_{233}, \lambda'_{223}, \lambda'_{232}, m_{\tilde{b}}, m_{\tilde{\nu}_\tau})$
- In a sense, $(\lambda', m_{\tilde{b}})$ and $(\lambda, m_{\tilde{\nu}_\tau})$ are orthogonal in our scenario since $(\lambda, m_{\tilde{\nu}_\tau})$ can only influence $(g-2)_\mu$ anomaly and 4-lepton constraint while on the other hand, $(\lambda', m_{\tilde{b}})$ can only influence $R_{D^{(*)}}$ and $R_{K^{(*)}}$ anomalies and other constraints (The influence to $(g-2)_\mu$ is very small because $m_{\tilde{b}}^2 \gg m_{\tilde{\nu}_\tau}^2$ as we will see from Fig(d)(e)(g)).
- So, we can plot the constraints and anomalies in two 2-D spaces: $(\lambda', m_{\tilde{b}})$ and $(\lambda, m_{\tilde{\nu}_\tau})$

Numerical scan

- We scan the 6-D parameter space $(\lambda_{232}, \lambda'_{233}, \lambda'_{223}, \lambda'_{232}, m_{\tilde{b}_{\rm R}} = m_{\tilde{b}_{\rm L}}, m_{\tilde{\nu}_\tau}, m_{\tilde{\tau}_{\rm L}} = 4\ \text{TeV})$
- $m_{\tilde{\nu}_\tau} \in [0.7, 1.2]$ TeV (also tried $m_{\tilde{\nu}_\tau} \in [1.2, 3]$ TeV but no solution found in this region)
- $|\lambda_{232}| \in [2.5, 3.5]$ (also tried $|\lambda_{232}| \in [1, 2.5]$ but no solution found in this region)
- $m_{\tilde{b}} \in [1.2, 10]$ TeV
- $|\lambda'_{233}| \in [0.01, 3]$
- $|\lambda'_{223}| \in [0.01, 3]$
- $|\lambda'_{232}| \in [0.01, 3]$
- 30 million attempts $\Rightarrow$ 1570 solutions (red+yellow+blue+green points)

Numerical scan

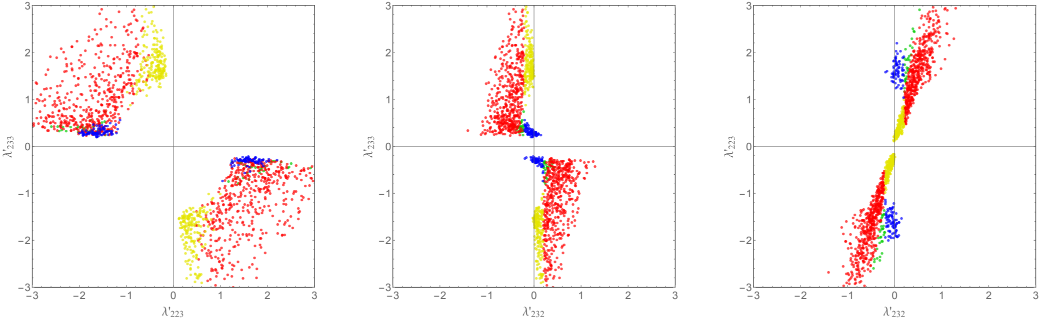

- Separate to 3 characteristically regions according to Fig(c). Yellow: $|\lambda'_{232}| < 0.2$ and $|\lambda'_{223}| < 1$; Blue: $|\lambda'_{232}| < 0.2$ and $|\lambda'_{223}| > 1$; Red: $|\lambda'_{232}| > 0.2$ and $1.5 < \frac{\lambda'_{223}}{\lambda'_{232}} < 5.5$
- From Fig(c), Red: $\frac{\lambda'_{223}}{\lambda'_{232}} \sim 3 \Leftarrow B_s - \overline{B}_s$ mixing. Green: crossover region from Red to Blue.
- Yellow+Blue: $|\lambda'_{232}|$ small or even zero. Fig(a-c): $|\lambda'_{233}\lambda'_{223}|$ small $\Leftarrow B_s - \overline{B}_s$ mixing.

Numerical scan

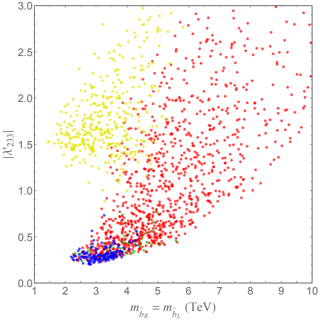

(d)

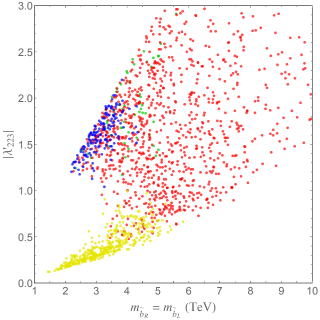

(e)

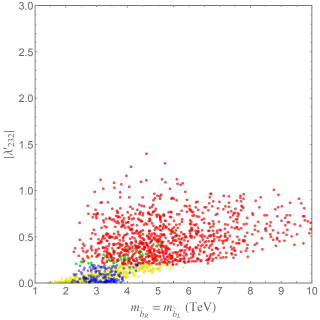

(f)

- Fig(a-c): the absolute sign of λ' not important, only the relative sign matters.
- Fig(e): $\frac{|\lambda'_{223}|}{(m_{\tilde{b}}/1\ \text{TeV})} \lesssim 0.57 \Leftarrow D^0 \to \mu^+\mu^-$; Fig(d): $\frac{|\lambda'_{233}|}{(m_{\tilde{b}}/1\ \text{TeV})} \lesssim 1.0$
- $\Rightarrow$ cannot contribute to $(g-2)_\mu$ much.
- Fig(h): $|\lambda'_{232}| \lesssim 1.5 \Leftarrow$ from Fig(c), $|\lambda'_{232}|$ is either small or $\sim |\lambda'_{223}|/3$

Numerical scan

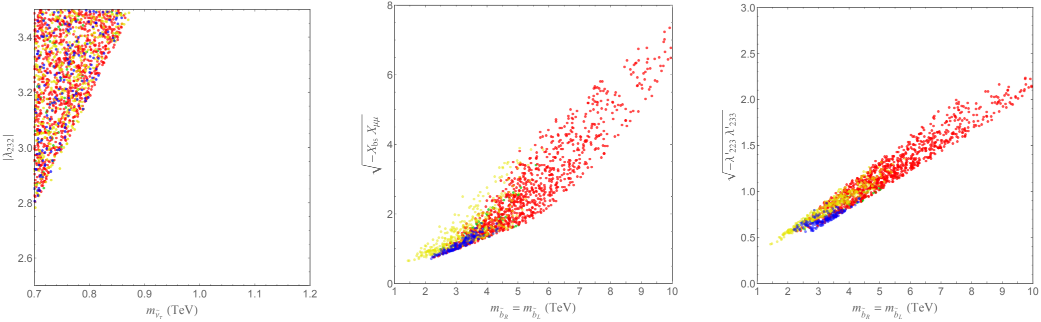

(g) (h) (i)

- Fig(g): Red, Yellow, Blue and Green points are totally mixed $\Leftarrow$ Orthogonality of the two 2-D subspaces: $(\lambda, m_{\tilde{\nu}_\tau})$ and $(\lambda', m_{\tilde{b}})$.
- Fig(h) $\Leftarrow R_{K^{(*)}} \Leftarrow \lambda'_{233}\lambda'_{223} < 0 \Leftarrow$ Fig(a)
- Fig(i): $\frac{\sqrt{-\lambda'_{223}\lambda'_{233}}}{(m_{\tilde{b}}/1\ \text{TeV})} \sim (0.2, 0.28) \Leftarrow B \to K\nu\bar{\nu}$

Numerical scan

- Fig(g) $\Rightarrow |\lambda_{232}| \gtrsim 2.78$
- Fig(g) $\Rightarrow 0.70 \text{ TeV} \lesssim m_{\tilde{\nu}_\tau} \lesssim 0.87 \text{ TeV}$
- Fig(d) $\Rightarrow |\lambda'_{233}| \gtrsim 0.20$
- Fig(e) $\Rightarrow |\lambda'_{223}| \gtrsim 0.12$
- Fig(f) $\Rightarrow |\lambda'_{232}|$ could be very small or even zero
- Fig(d-f) $\Rightarrow m_{\tilde{b}} \gtrsim 1.44 \text{ TeV}$
- Fig(g) $\Rightarrow \frac{|\lambda_{232}|}{(m_{\tilde{\nu}_\tau}/1 \text{ TeV})} \gtrsim 4$; Fig(d) $\Rightarrow \frac{|\lambda'_{233}|}{(m_{\tilde{b}_R}/1 \text{ TeV})} \lesssim 1$; Fig(e) $\Rightarrow \frac{|\lambda'_{223}|}{(m_{\tilde{b}_R}/1 \text{ TeV})} \lesssim 0.57$. This means that the sneutrino term gives the main contribution of muon (g-2) as one can see from Eq.(3).

Benchmark scenarios

- Density/number of the points in some region $\propto$ the size of the allowed region of the parameter space.
- Three benchmark scenarios:
  - Red scenario (a subset of the Red region in the scatter plot): $\lambda'_{233} = -\lambda'_{223} = -3\lambda'_{232}$, $m_{\tilde{b}_R} = m_{\tilde{b}_L}$, $m_{\tilde{\tau}_L} = 4$ TeV. Fig(c): choose $\lambda'_{223} = -3\lambda'_{232}$ to collect as many red points as possible.
  - Yellow scenario (a subset of the Yellow region in the scatter plot): $\lambda'_{233} = -8\lambda'_{223}$, $\lambda'_{232} = 0$, $m_{\tilde{\tau}_L} = 4$ TeV. Fig(a): $\lambda'_{233} = -8\lambda'_{223}$ to collect as many yellow points as possible.
  - Blue scenario (a subset of the Blue region in the scatter plot): $\lambda'_{223} = -6\lambda'_{233}$, $\lambda'_{232} = 0$, $m_{\tilde{\tau}_L} = 4$ TeV. Fig(a): $\lambda'_{223} = -6\lambda'_{233}$ to collect as many blue points as possible.
  * Red scenario, $\lambda'_{233} = -\lambda'_{223}$ for simplicity.
  * Yellow & Blue scenario, $\lambda'_{232} = 0$ for simplicity $\Rightarrow m_{\tilde{b}_L}, m_{\tilde{t}_L}$ will not appear.

Collider signals

- Signal for $(\lambda', m_{\tilde{b}})$ space: $pp \to \bar{t}\mu^+\mu^-$

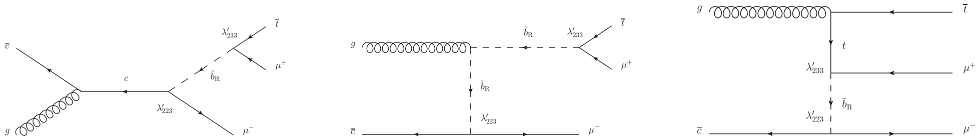

(j) (k) (l)

  - $p_T^{t,\mu} > 20$ GeV, $|\eta^{t,\mu}| < 2.5$, $\Delta R^{\mu\mu} > 0.4$ and $\Delta R^{t\mu} > 0.4$, $M_{\mu^+\mu^-} > 0.4$ TeV. Assume $\mathscr{L} = 3000\ \mathrm{fb}^{-1}$. $\sqrt{s} = 14\ \mathrm{TeV}, 27\ \mathrm{TeV}, 100\ \mathrm{TeV}$.
  - Background small. $pp \to \bar{t}\mu^+\mu^- X$ (with $X = j, b, W^+ \to jj, W^+ \to \ell^+\nu_\ell$ not detected: $p_T^{j,b,l} < 20$ GeV, $E_T^{\mathrm{miss}} < 20$ GeV)
  - $pp \to t\mu^+\mu^-$ is similar but with a larger background.
  - Only λ'_{233}, λ'_{223} and $m_{\tilde{b}_R}$ contribute to the signal. What can be probed are actually these parameters, a projection of the scenario.

Collider signals

- Signal for $(\lambda, m_{\tilde{\nu}_\tau})$ space: $pp \to \mu^+\mu^-\mu^+\mu^-$

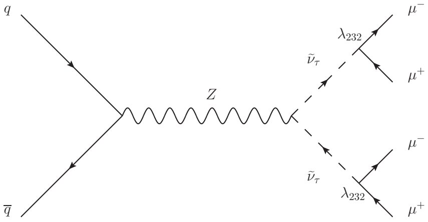

(m)

- $p_T^\mu > 25$ GeV, $|\eta^\mu| < 2.47$, $\Delta R^{\mu\mu} > 0.2$, $M_{\mu^+\mu^-} > 0.4$ TeV.
- Assume the mass of the lightest neutralino is 100 GeV for the calculation of the branching ratio of $\tilde{\nu}_\tau$. $\mathrm{BR}(\tilde{\nu}_\tau \to \mu^+\mu^-)$ is larger than 95% when $|\lambda_{232}| > 1.2$

Anomalies and constraints (Red scenario)

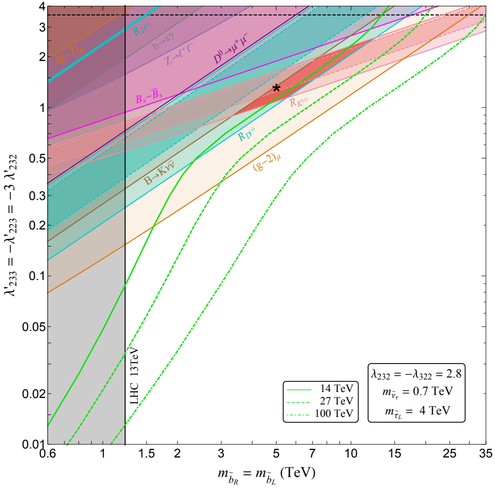

(n)

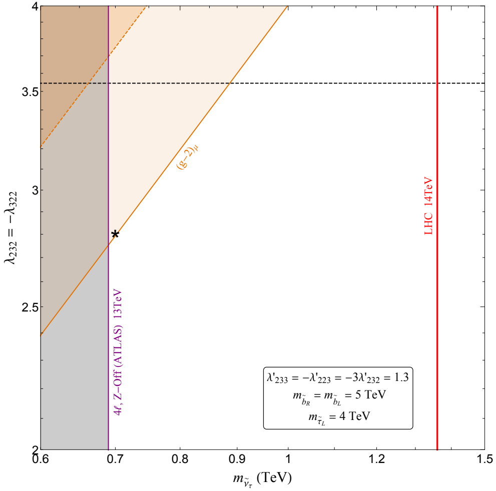

(o)

Anomalies and constraints (Yellow scenario)

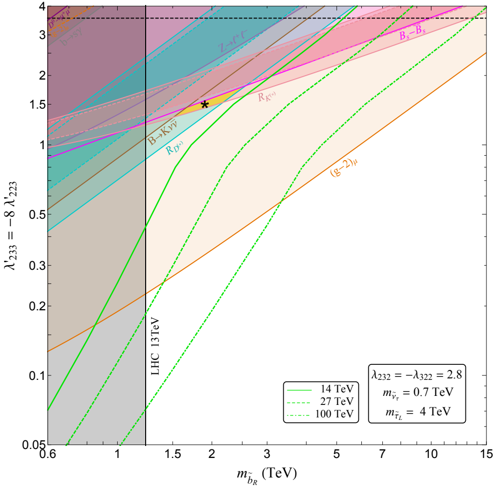

(p)

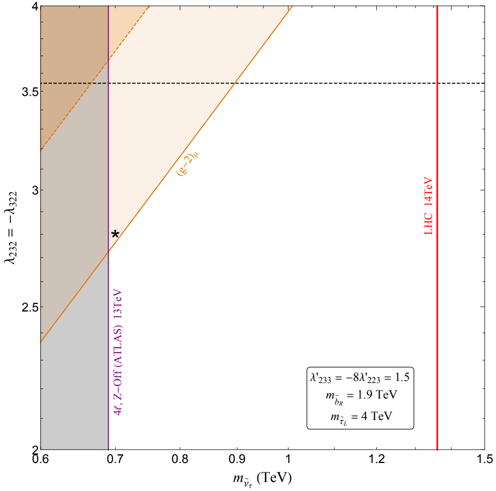

(q)

Anomalies and constraints (Blue scenario)

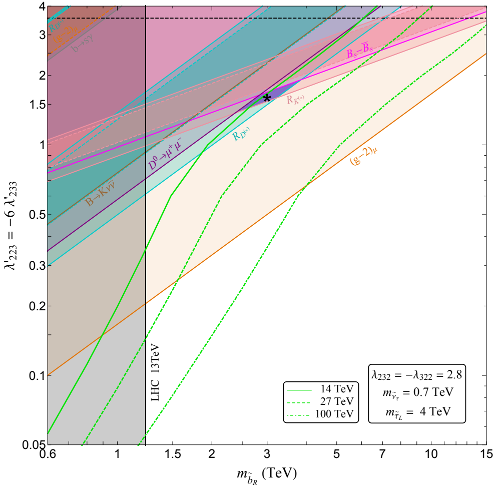

(r)

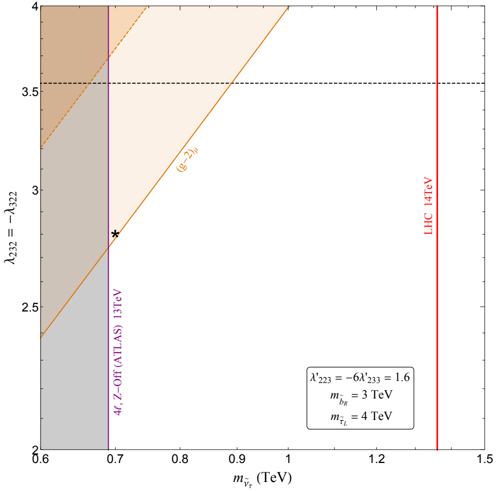

(s)

Discussions

- The figure on the left uses the value of the black star in the figure on the right and vice versa.
- The cyan, pink and orange shaded regions with solid (dashed) boundaries explain the $R_{D^{(*)}}$, $R_{K^{(*)}}$ and $(g-2)_\mu$ anomalies at 3σ (2σ) CL respectively.
- The red, yellow and blue shaded regions are the overlap regions that simultaneously explain all the three anomalies correspond to the red, yellow and blue scenarios.
- The green solid, dashed and dot-dashed lines in Fig(n)(p)(r) are the 2σ sensitivities of the $\sqrt{s} =$ 14 TeV, 27 TeV and 100 TeV pp colliders in the $\bar{t}\mu^+\mu^-$ channel.
- These green curves bend downward at large λ' region because of the off-shell contribution of $pp \to \bar{t}\mu^+\mu^-$ Fig(l).
- The red solid line in Fig(o)(q)(s) are the 2σ sensitivities of the LHC 14 TeV in the 4-muon channel.
- Fig(o)(q)(s) are quite similar. Consistent with Fig(g). Consequence of the orthogonality of the two subspaces $(\lambda, m_{\tilde{\nu}_\tau})$ and $(\lambda', m_{\tilde{b}})$

Discussions

- In the yellow and blue scenarios, we can allow a non-zero λ'_{232} (correspond to the yellow and blue points out of the vertical axis in Fig(b,c)). And this will make the $B_s - \overline{B}_s$ mixing constraint weaker and enlarge the allowed parameter space for $R_{K^{(*)}}$.
- We choose the black stars that are very close to the 3σ lower bound of $(g-2)_\mu$ in Fig(o)(q)(s) to show the dependence of $(g-2)_\mu$ from $(\lambda', m_{\widetilde{b}})$ in Fig(n)(p)(r). Otherwise, the 3σ lower bound of $(g-2)_\mu$ will disappear in Fig(n)(p)(r) because the contribution from $\widetilde{b}$ is much smaller compared with $\widetilde{\nu}_\tau$.
- $B_s \to \mu^+\mu^-$ is always satisfied once $R_{K^{(*)}}$ is explained. Even if we take the extreme 3σ value, $|(C_{10})^\mu - (C'_{10})^\mu| = 0.89$ (Altmannshofer, Stangl (arXiv:2103.13370)). This implies the RPV contribution $< 1.4 \times 10^{-10}$ (Becirevic, Fajfer, Kosnik (PRD 2015)) while the current experimental value is BR$(B_s \to \mu^+\mu^-) = (3.0 \pm 0.4) \times 10^{-9}$
- The lower bound of $m_{\widetilde{\nu}_\tau}$ comes from the recast of the 4-lepton search of ATLAS (ATLAS-CONF-2021-011). The 4-lepton signal in our scenario comes from the pair production of $\widetilde{\nu}_\tau$ with $\widetilde{\nu}_\tau \to \mu^+\mu^-$.

Summary

- We suggest that in RPV3 SUSY:
  - A $\tilde{b}$ with mass $\sim 2 - 12$ TeV and non-zero couplings λ'_{233}, λ'_{223} and λ'_{232} could explain $R_{D^{(*)}}$ and $R_{K^{(*)}}$ anomalies at 3σ CL (especially even 1σ for $R_{K^{(*)}}$) while having a little bit contribution on $(g-2)_\mu$ anomaly due to the constraints of $B \to K^{(*)}\nu\overline{\nu}$, $B_s - \overline{B}_s$ mixing etc.;
  - A $\tilde{\nu}_\tau$ with mass $\sim 0.7 - 1$ TeV and non-zero coupling $|\lambda_{232}| \gtrsim 2.7$ could explain $(g-2)_\mu$ anomaly at 3σ CL.
  - Both $(m_{\tilde{b}}, \lambda')$ and $(m_{\tilde{\nu}_\tau}, \lambda)$ parameter spaces are (partly) testable at HL-LHC through $\bar{t}\mu^+\mu^-$ or four muon signals.
  - Due to the orthogonality between $(m_{\tilde{b}}, \lambda')$ and $(m_{\tilde{\nu}_\tau}, \lambda)$ in the sense of the solutions of anomalies, even if the $(m_{\tilde{b}}, \lambda')$ solution is ruled out by the signal we proposed or future low energy constraints, the $(m_{\tilde{\nu}_\tau}, \lambda)$ solution is still valid and vice versa.

Backup

Choice of the couplings

- $(g-2)_\mu \Rightarrow$ candidates from Eq.(3): $\lambda_{312}, \lambda_{321}, \lambda_{322}, \lambda_{323}$ (λ'_{2k3} terms cannot contribute much). To get enough contribution, we have to let at least two λ couplings to be non-zero otherwise the magnitude of the λ need to be larger than $\sqrt{4\pi}$.
- ✓ $\lambda_{322} \neq 0$, contributes two times for $k = 2$ in Eq.(3)
- $\times$ $\lambda_{323} \neq 0$, need to add another coupling to get enough contribution. But $\tau \to \bar{e}\mu\mu \Rightarrow \lambda_{323}\lambda_{312}$ small (propagator $\widetilde{\nu}_\tau$); $\tau \to e\mu\bar{\mu} \Rightarrow \lambda_{323}\lambda_{321}$ small (propagator $\widetilde{\nu}_\tau$); $\tau \to \mu\mu\bar{\mu} \Rightarrow \lambda_{323}\lambda_{322}$ small (propagator $\widetilde{\nu}_\tau$).
- ? $\lambda_{312} \neq 0$ and $\lambda_{321} \neq 0$, cannot let $\lambda_{322} \neq 0$ at the same time due to the constraint of $\mu \to e\gamma$
- $\times$ $\lambda'_{3ij} \neq 0$ moreover, because $(\bar{d}_i d_j) \to \mu\bar{\mu} \Rightarrow \lambda_{322}\lambda'_{3ij}$ small (propagator $\widetilde{\nu}_\tau$).

Choice of couplings

- $R_{K^{(*)}} \Rightarrow \lambda'_{233}\lambda'_{223} \neq 0$ since $\lambda'_{3ij} \approx 0$ and $\lambda_{323} \approx 0$
- $\checkmark$ $\lambda'_{233} \neq 0$ and $\lambda'_{223} \neq 0$. Only choice of $R_{K^{(*)}}$, also contribute to $R_{D^{(*)}}$
- $\lambda'_{ij3} \neq 0$ and $\lambda'_{i3j} \neq 0$ may cause some troubles because
  $(\overline{u}_j c) \to \overline{e}_i \mu \Rightarrow \lambda'_{223}\lambda'_{ij3}$ (propagator $\widetilde{b}_{\rm R}$) e.g. $D^0 \to \mu^+\mu^- \Rightarrow \frac{\lambda'_{213}}{m^2_{\tilde{b}_{\rm R}}}$ small;
  $(\overline{d}_j b) \to \overline{e}_i \mu \Rightarrow \lambda'_{233}\lambda'_{i3j}$ (propagator $\widetilde{t}_{\rm L}$) e.g. $B_s \to \mu^+\mu^- \Rightarrow \frac{\lambda'_{232}}{m^2_{\tilde{t}_{\rm L}}}$ small.
- In our case $\lambda'_{232} \neq 0$. But a small λ'_{232} may also be possible (but the cancellation term in $B_s - \overline{B}_s$ mixing is zero) and λ'_{232} will contribute to $B_s \to \mu^+\mu^-$, $(C'_9)^\mu$ and $(C'_{10})^\mu$. But λ'_{232} do not have to be small and prefer the relation $\lambda'_{223} \approx 3\lambda'_{232}$.
- Now, non-zero couplings are chosen to be λ_{232}, λ'_{233}, λ'_{223} and λ'_{232}.

Background cross-section

- $pp \to t\mu^+\mu^-$ has a larger background cross-section because the u content in proton is much larger than the $\overline{u}$ content.
- We can look for $t\mu^+\mu^-$ or even combine both, but the result should be similar because the signal of $t\mu^+\mu^-$ is nearly the same as $\bar{t}\mu^+\mu^-$.

Table 1: $pp \to \bar{t}\mu^+\mu^- X$ cross sections (fb)

X	14 TeV	$M_{\mu^+\mu^-} > 0.15$ TeV	27 TeV	$M_{\mu^+\mu^-} > 0.15$ TeV	100 TeV	$M_{\mu^+\mu^-} > 0.15$ TeV
j	0.381	3.35×10^{-3}	1.06	1.05×10^{-2}	5.83	7.11×10^{-2}
b	4.23×10^{-3}	3.64×10^{-5}	9.47×10^{-3}	9.85×10^{-5}	3.84×10^{-2}	3.92×10^{-4}
$W^+ \to jj$	3.76×10^{-3}	2.75×10^{-5}	1.49×10^{-2}	1.33×10^{-4}	0.133	1.58×10^{-3}
$W^+ \to e^+\nu_e$	6.38×10^{-4}	5.68×10^{-6}	2.53×10^{-3}	2.68×10^{-5}	2.24×10^{-2}	2.28×10^{-4}
$W^+ \to \mu^+\nu_\mu$	6.15×10^{-3}	2.67×10^{-3}	2.64×10^{-2}	1.12×10^{-2}	0.242	0.120
$W^+ \to \tau^+\nu_\tau$	6.34×10^{-4}	6.09×10^{-6}	2.52×10^{-3}	3.08×10^{-5}	2.25×10^{-2}	2.81×10^{-4}
Total	0.396	6.10×10^{-3}	1.12	2.20×10^{-2}	6.29	0.194

[a] $p_T^{j,b,l} < 20$ GeV, $E_T^{miss} < 20$ GeV
[b] $p_T^{t,\mu} > 20$ GeV, $|\eta^{t,\mu}| < 2.5$

Invariant mass distribution (Red scenario)

- For the process $pp \to \bar{t}\mu^+\mu^-$
- Invariant mass $M_{\mu^+\mu^-}$ distributions at $\sqrt{s} = 14\ \mathrm{TeV}, 27\ \mathrm{TeV}, 100\ \mathrm{TeV}$

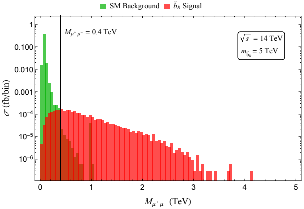

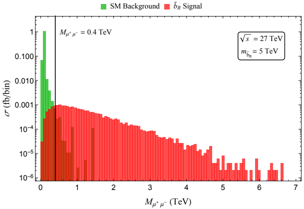

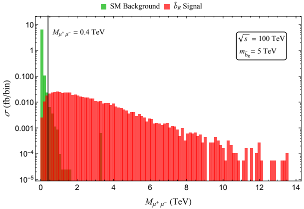

- We have used $\lambda'_{233} = -\lambda'_{223} = 1.3$, $m_{\tilde{b}_R} = 5\ \mathrm{TeV}$ for the signal process (the black star in Fig(n)).

Invariant mass distribution (Yellow scenario)

- For the process $pp \to \bar{t}\mu^+\mu^-$
- Invariant mass $M_{\mu^+\mu^-}$ distributions at $\sqrt{s} = 14\ \mathrm{TeV}, 27\ \mathrm{TeV}, 100\ \mathrm{TeV}$

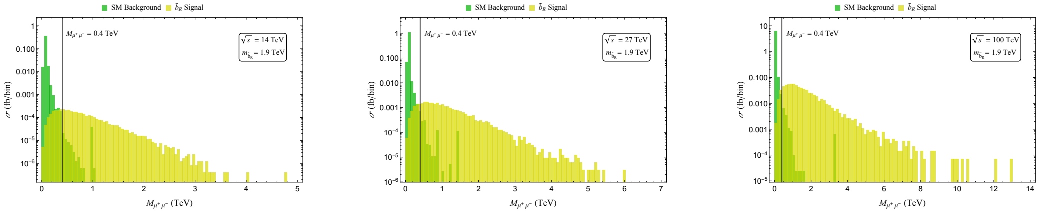

- We have used $\lambda'_{233} = -8\lambda'_{223} = 1.5$, $m_{\tilde{b}_R} = 1.9\ \mathrm{TeV}$ for the signal process (the black star in Fig(p)).

Invariant mass distribution (Blue scenario)

- For the process $pp \to \bar{t}\mu^+\mu^-$
- Invariant mass $M_{\mu^+\mu^-}$ distributions at $\sqrt{s} = 14\ \mathrm{TeV}, 27\ \mathrm{TeV}, 100\ \mathrm{TeV}$

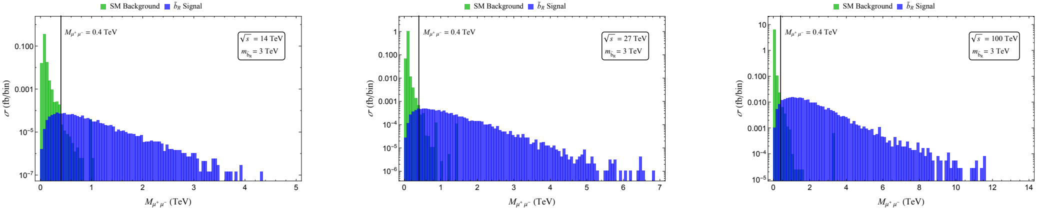

- We have used $\lambda'_{223} = -6\lambda'_{233} = 1.6$, $m_{\tilde{b}_R} = 3\ \mathrm{TeV}$ for the signal process (the black star in Fig(r)).

Anomalies and constraints (Red scenario)

- Since many anomalies and constraints are independent of $(\lambda_{232}, m_{\tilde{\nu}_\tau})$, they become just numbers instead of curves in Fig(o).

Anomaly/Constraint	Quantities in Figure(m)	Experimental value/limit
$R_{D^{(*)}}$	$\frac{R_{D^{(*)}}}{R^{\text{SM}}_{D^{(*)}}} = 1.05$	1.15 ± 0.04
$R_{K^{(*)}}$	$(C_9)^\mu = -(C_{10})^\mu = -0.23$	-0.35 ± 0.08
$D^0 \to \mu^+\mu^-$	$\text{BR}(D^0 \to \mu^+\mu^-) = 2.8 \times 10^{-10}$	$< 7.6 \times 10^{-9}$ (95% CL)
$B \to K^{(*)}\nu\overline{\nu}$	$R_{B\to K^{(*)}\nu\overline{\nu}} = \frac{\text{BR}(B\to K^{(*)}\nu\overline{\nu})}{\text{BR}_{\text{SM}}(B\to K^{(*)}\nu\overline{\nu})} = 4.6$	< 5.2 (95% CL)
$B_s - \overline{B}_s$ mixing	$\Delta M_{B_s} = (20.1 \pm 1.7)\ \text{ps}^{-1}$	$(17.757 \pm 0.021)\ \text{ps}^{-1}$
$B_s \to \mu^+\mu^-$	$< 9.1 \times 10^{-12}$	$(3.0 \pm 0.4) \times 10^{-9}$

Anomalies and constraints (Yellow scenario)

- Since many anomalies and constraints are independent of $(\lambda_{232}, m_{\tilde{\nu}_\tau})$, they become just numbers instead of curves in Fig(q).

Anomaly/Constraint	Quantities in Figure(o)	Experimental value/limit
$R_{D^{(*)}}$	$\frac{R_{D^{(*)}}}{R^{\rm SM}_{D^{(*)}}} = 1.04$	1.15 ± 0.04
$R_{K^{(*)}}$	$(C_9)^\mu = -(C_{10})^\mu = -0.13$	-0.35 ± 0.08
$D^0 \to \mu^+\mu^-$	$\mathrm{BR}(D^0 \to \mu^+\mu^-) = 2.6 \times 10^{-12}$	$< 7.6 \times 10^{-9}$ (95% CL)
$B \to K^{(*)}\nu\overline{\nu}$	$R_{B\to K^{(*)}\nu\overline{\nu}} = \frac{\mathrm{BR}(B\to K^{(*)}\nu\overline{\nu})}{\mathrm{BR}_{\rm SM}(B\to K^{(*)}\nu\overline{\nu})} = 3.3$	< 5.2 (95% CL)
$B_s - \overline{B}_s$ mixing	$\Delta M_{B_s} = (22.4 \pm 1.7)\ \mathrm{ps}^{-1}$	$(17.757 \pm 0.021)\ \mathrm{ps}^{-1}$
$B_s \to \mu^+\mu^-$	3.0×10^{-12}	$(3.0 \pm 0.4) \times 10^{-9}$

Anomalies and constraints (Blue scenario)

- Since many anomalies and constraints are independent of $(\lambda_{232}, m_{\tilde{\nu}_\tau})$, they become just numbers instead of curves in Fig(s).

Anomaly/Constraint	Quantities in Figure(q)	Experimental value/limit
$R_{D^{(*)}}$	$\frac{R_{D^{(*)}}}{R^{\rm SM}_{D^{(*)}}} = 1.03$	1.15 ± 0.04
$R_{K^{(*)}}$	$(C_9)^\mu = -(C_{10})^\mu = -0.13$	-0.35 ± 0.08
$D^0 \to \mu^+\mu^-$	$\mathrm{BR}(D^0 \to \mu^+\mu^-) = 5.4 \times 10^{-9}$	$< 7.6 \times 10^{-9}$ (95% CL)
$B \to K^{(*)}\nu\overline{\nu}$	$R_{B\to K^{(*)}\nu\overline{\nu}} = \frac{\mathrm{BR}(B\to K^{(*)}\nu\overline{\nu})}{\mathrm{BR_{SM}}(B\to K^{(*)}\nu\overline{\nu})} = 1.3$	< 5.2 (95% CL)
$B_s - \overline{B}_s$ mixing	$\Delta M_{B_s} = (22.2 \pm 1.7)\ \mathrm{ps}^{-1}$	$(17.757 \pm 0.021)\ \mathrm{ps}^{-1}$
$B_s \to \mu^+\mu^-$	2.8×10^{-12}	$(3.0 \pm 0.4) \times 10^{-9}$